



## Research Article

# Effect of Biosynthesized Silver Nanoparticles on the Properties of Chemically Modified *Agave tequilana* Weber var. Azul Fibers

Arahí Alvarado-Arámburo,<sup>1</sup> Gilberto Velázquez,<sup>1</sup> Margarita Cid Hernández <sup>1</sup>,  
Oscar-Kevin Reyes,<sup>1</sup> Luis J. González-Ortiz,<sup>2</sup> Ricardo H. Cruz-Estrada,<sup>1</sup>  
Milton O. Vázquez-Lepe,<sup>1</sup> Jaime A. Jimenez-Aguilar,<sup>3</sup> José Navarro-Partida,<sup>1</sup>  
and Edgar J. López-Naranjo <sup>1</sup>

<sup>1</sup>CUCEI, Universidad de Guadalajara, 44430 Guadalajara, Jal, Mexico

<sup>2</sup>CICY, 97205 Mérida, Yuc, Mexico

<sup>3</sup>Tecnológico de Monterrey, Escuela de Medicina y Ciencias de la Salud, Monterrey 64849, Mexico

Correspondence should be addressed to Edgar J. López-Naranjo; [edgar.lopezn@academicos.udg.mx](mailto:edgar.lopezn@academicos.udg.mx)

Received 17 March 2022; Revised 13 June 2022; Accepted 22 June 2022; Published 9 July 2022

Academic Editor: Nagamalai Vasimalai

Copyright © 2022 Arahí Alvarado-Arámburo et al. This is an open access article distributed under the Creative Commons Attribution License, which permits unrestricted use, distribution, and reproduction in any medium, provided the original work is properly cited.

*Agave tequilana* Weber var. azul fibers (ATF) are widely used as a reinforcement material despite their polarity makes them incompatible with hydrophobic matrices. Consequently, ATF are commonly modified employing different chemical processes (e.g., mercerization and coupling agents) to change their surface characteristics to improve the interface between the fibers and the polymeric matrix. Nevertheless, these treatments could damage the fibers during the process, negatively affecting their natural properties. The use of nanotechnology to repair this natural material could help to restore its intrinsic properties and give it new ones as antibacterial activity. In this work, chemically treated ATF were used as templates for the biosynthesis of silver nanoparticles (AgNPs) using a natural extract obtained from *Agave tequilana* Weber var. azul leaves (ATL) as reducing agent. Scanning and transmission electron microscopy images as well as dynamic light scattering results indicate that stable nanometric particles were successfully synthesized on all fibers. X-ray photoelectron spectroscopy and X-ray diffraction results confirm the composition of the nanoparticles. Tensile tests indicate that AgNPs improved the mechanical properties of fibers previously mercerized and treated with maleic anhydride grafted polyethylene as coupling agent. Additionally, an antibacterial effect against *S. enterica* was conferred to ATF due to the presence of AgNPs.

## 1. Introduction

Natural fibers are widely used as a reinforcement material in different kinds of composite materials (e.g., wood plastic composites (WPC)) despite lignocellulosic fibers are incompatible with hydrophobic matrices due to their polarity [1, 2]. To enhance the poor interaction between natural fibers and hydrophobic matrices, different chemical treatments are employed (e.g., mercerization and coupling agents); as a result, the mechanical properties of the final product are improved due to a better interface between the fibers and the polymeric matrix. Mercerization consists in immersing fibers in an alkaline solution removing pectin, waxy sub-

stances, and natural oils present on the surface layer of the fibers. Subsequently, a rougher surface with a more porous structure is produced. However, it could decrease the mechanical properties of natural fibers due to fibrillation. Mercerization is frequently used as a pretreatment to increase the efficiency of any further chemical treatment (e.g., coupling agents). Coupling agents are easier to handle than alternative methods used to improve the interfacial bonding between wood and thermoplastics. Coupling agents chemically interact with natural fibers and mechanically with the hydrophobic matrices enhancing the compatibility and consequently achieving a better interfacial bonding [2–6].

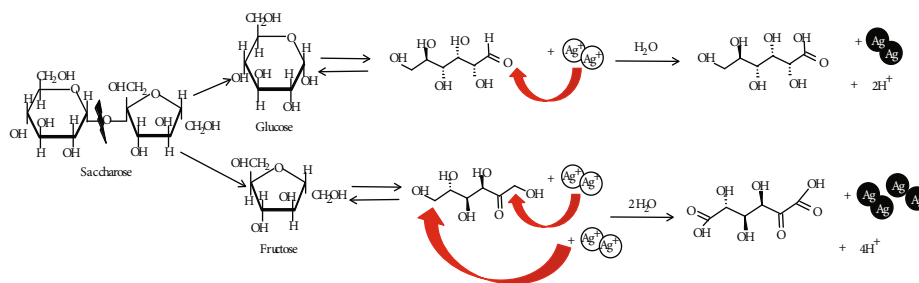


FIGURE 1: Proposed chemical reaction to produce AgNPs using ATE as reducing agent.

On the other hand, during the last two decades, metallic nanoparticle (MNP) research has increased due to the wide range of properties that make them suitable for different applications [7]. Among the available synthesis methods, green routes constitute cost-effective and environmentally friendly alternatives to traditional processes (i.e., chemical and physical) used to obtain MNPs. Particularly, plant-mediated methods offer potential benefits due to the absence of toxic chemicals, nonbiological risk, low cost of production, and the use of natural capping and reducing agents [8–11]. Currently, a wide variety of plant extracts have been successfully used in the synthesis of metallic nanoparticles due to the presence of different phytochemicals and biopolymers that act as reducing agents (e.g., polysaccharides, terpenoids, flavonoids, phenolic compounds, saponins, and lignocellulosic materials). Although the mechanistic aspects of the green synthesis process are still unknown, it has been reported that phytochemicals reduce metallic ions through functional groups such as  $-\text{CO}$ ,  $-\text{OH}$ , and  $-\text{NH}$  present at their constituent molecules [10]. A possible chemical reaction on how silver nanoparticles (AgNPs) could be produced using *Agave tequilana* Weber var. azul extract (ATE) is proposed and described in Figure 1. As a part of the synthesis process to obtain AgNPs,  $\text{Ag}^+$  must be reduced to  $\text{Ag}^0$  in the presence of reducing molecules. To do so, sucrose present in *Agave tequilana* Weber var. azul leaves (ATL) needs to be hydrolyzed to obtain glucose and fructose. Glucose belongs to the family of aldoses, which are characterized by the presence of an aldehyde group, which in the presence of  $\text{Ag}^+$ , water and heating promotes the oxidation of carbon up to the formation of a carboxylic acid group, releasing two hydrogen protons ( $\text{H}^+$ ) and the reduction of silver ( $\text{Ag}^0$ ) to obtain AgNPs. An alternative process would be focused on the reducing molecule fructose, which belongs to the ketose family. The ketone's carbon in contrast to the aldehyde's carbon is at its maximum degree of oxidation, which nulls out the possibility that  $\text{Ag}^+$  could oxidize this carbon, as well as the possibility that this substrate could be the first oxidized molecule during the synthesis of nanoparticles. However, in contrast to glucose, fructose shows two terminal  $-\text{OH}$  groups, which can be more easily oxidized. From this analysis, it is proposed that during  $\text{Ag}^+$  reduction process, for each glucose oxidized, two  $\text{Ag}^0$  nanoparticles can be reduced, and once glucose is no longer available in the media, fructose will be now oxidized.

Among different MNPs, AgNPs have caught the world's attention due to their novel chemical, physical, and biologi-

cal properties. So far, green synthesized AgNPs have been used in pharmacological applications and wastewater treatment, as well as in the cosmetic, textile, and food industry [12–14]. However, potential applications of AgNPs in the development of new lignocellulosic composite materials have been scarcely studied despite the incorporation of AgNPs could improve the mechanical properties of natural fibers commonly used as reinforcement material in lignocellulosic composites and confer them new properties, expanding their possible applications [15–21]. Thus, in this work, the effect of biosynthesized AgNPs on the tensile properties and antibacterial activity of chemically surface-modified *Agave tequilana* Weber var. Azul fibers (ATF) is reported.

## 2. Materials and Methods

The materials are as follows:  $\text{AgNO}_3$  (Sigma-Aldrich),  $\text{NaOH}$  (Lavoisier-Chem), maleic anhydride grafted polyethylene, (MAPE; DuPont), and xylene (Golden-Bell). *Agave tequilana* Weber var. azul plant was purchased from a nursery in Tequila-Mexico. ATF were donated by a tequila company of the Mexican state of Jalisco, Mexico. Experimental research and collection of plant material were performed in accordance with relevant institutional, national, and international guidelines and regulations.

### 2.1. Fiber Preparation

**2.1.1. Agave Fiber Pretreatment.** Fibers were soaked in water and washed repeatedly until all impurities were eliminated; subsequently, fibers were dried outdoors and manually separated. In a second stage, fibers were milled and sieved; untreated fibers (UF) retained on mesh 50 were collected for subsequent treatments.

**2.1.2. Mercerization.** Mercerized fibers (MF) were obtained soaking UF in a 2 wt%  $\text{NaOH}$  aqueous solution (fibers/solution wt. ratio: 1/10) at room temperature for 30 min. After this process, fibers were repeatedly washed and dried outdoors.

**2.1.3. Coupling Agent Treatment.** Mercerized fibers treated with MAPE (MMF) were obtained treating MF with a MAPE solution in xylene (3 wt%; fibers/xylene wt. ratio: 1/20) at  $90^\circ\text{C}$  during 30 min. After MAPE treatment, fibers were removed from the solution and dried at room temperature in an extraction hood.

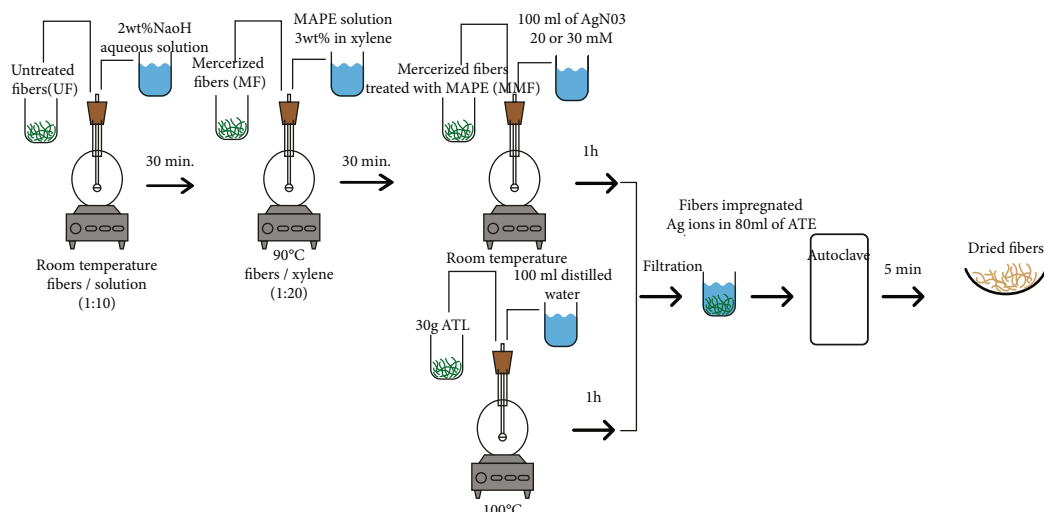


FIGURE 2: Illustration of the synthesis process.

TABLE 1: Tensile properties of unmodified and modified ATF.

Sample code	Treatment			Strength (se) $\times 10^{-2}$ , in MPa	Modulus (se) $\times 10^{-3}$ , in MPa
	Mercerization	Coupling agent addition	AgNO <sub>3</sub> concentration		
UF	—	—	—	1.4 (0.2)	4.9 (0.5)
UF/20	—	—	20 mM	1.4 (0.4)	5.5 (1.6)
UF/30	—	—	30 mM	1.7 (0.3)	6.2 (1.3)
MF	x	—	—	1.1 (0.1)	4.2 (0.3)
MF/20	x	—	20 mM	1.1 (0.1)	4.2 (0.4)
MF/30	x	—	30 mM	1.1 (0.1)	5.5 (0.7) <sup>a</sup>
MMF	x	x	—	1.3 (0.2)	4.6 (0.5)
MMF/20	x	x	20 mM	1.5 (0.1)	6.0 (0.4) <sup>a</sup>
MMF/30	x	x	30 mM	2.5 (0.3) <sup>a</sup>	10.0 (2.1) <sup>a</sup>

UF: untreated fibers; MF: mercerized fibers; MMF: mercerized fibers treated with MAPE. x indicates that a specific treatment was applied to the sample. se: standard error. <sup>a</sup> $p < 0.05$ .

### 3. Synthesis of AgNPs Using ATF as Template

**3.1. Preparation of ATE.** ATL were washed, cut and boiled (30 g/100 mL of distilled water) for 1 h. The solution was filtered to remove solid residues.

**3.2. AgNP Synthesis Using ATF as Templates.** ATF (UF, MF, or MMF) were poured into 100 mL of AgNO<sub>3</sub> solution 20 mM (AgNPs20) or 30 mM (AgNPs30) during 1 h. Later, fibers were filtered to eliminate AgNO<sub>3</sub> solution excess. Fibers impregnated with Ag<sup>+</sup> ions were soaked in 80 mL of ATE and autoclaved during 5 min at 110°C. Finally, fibers were removed and dried at room temperature.

Figure 2 illustrates the process followed to obtain the testing samples analyzed in this work, which are listed in Table 1.

### 4. Characterization

Fourier-transform infrared spectroscopy: attenuated total reflectance spectroscopy was performed using a Nicolet

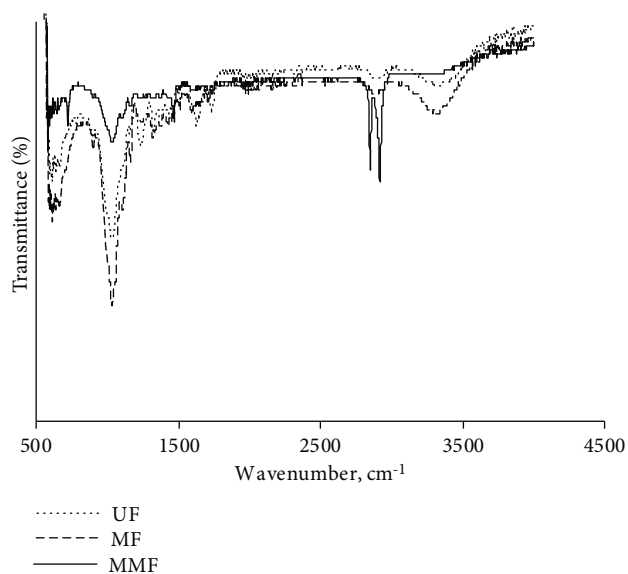


FIGURE 3: FTIR of UF, MF, and MMF.

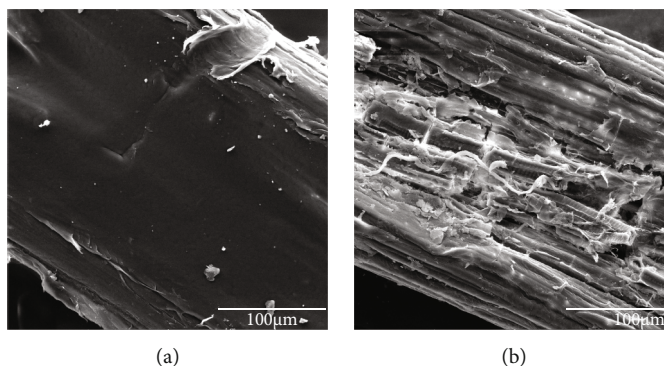


FIGURE 4: SEM images of (a) MMF and (b) MF.

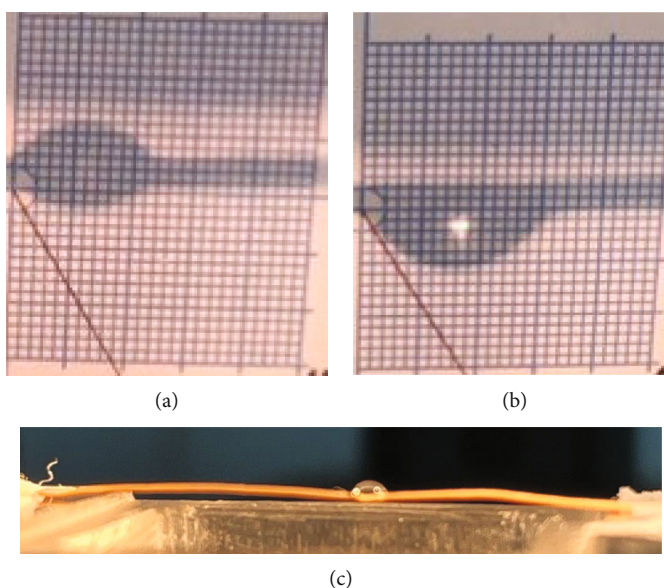


FIGURE 5: Contact angle images of (a) MF, (b) MMF, and (c) image of a droplet deposited on a fiber during contact angle tests.

iS50 FTIR. For each sample, 30 scans were recorded ( $4000\text{--}400\text{ cm}^{-1}$ ). Electron microscopy: SEM and TEM micrographs as well as energy dispersive X-ray spectroscopy (EDS) analysis were obtained using a scanning electron microscope FE-SEM TESCAN MIRA-3 LMU equipped with EDS operating at 20 kV and a JEOL JEM1010 microscope operating at 80 kV, respectively. Contact angle: to characterize the wetting behavior of fibers, contact angle was analyzed with a Tantec Contact Angle Meter model CAM-Micro taking TAPPI T458 test method as reference. Tests were performed at room temperature with at least five specimens per fiber. *X-ray diffraction*: XRD tests were performed using a Panalytical Empyrean device with Cu,  $\lambda = 1.54059\text{Å}$  operating at 40 kV and 30 mA, and the scanning range ( $2\theta$ ) from  $30^\circ$  to  $70^\circ$ . *X-ray photoelectron spectroscopy*: XPS tests were performed using an X-ray photoelectron spectrometer (PHOIBOS 150, SPECS Germany) with a monochromatic Al  $K_{\alpha}$  ( $h\nu = 1486.7\text{ eV}$ ) XR50M source operated at 250 W. Wide spectra were obtained using 1.0 eV of step size and 70 eV of pass energy. High-resolution spectra data of core levels

Ag3d, C1s, and O1s were collected using 0.1 eV step size and 15 eV pass energy. Higher resolution spectra of peaks were deconvoluted using software AAnalyzer<sup>1</sup> v2.21. The C1s spectra were fitted and adjusted with a corresponding shift using reference position at 284.8 eV due to adventitious carbon presented in sample. *Tensile testes*: tensile properties of ATF were evaluated using a universal machine Instron model 3345 according to ASTM C1557 test method using a crosshead speed of  $5\text{ mm min}^{-1}$  for five specimens of each sample.

*4.1. Antibacterial Activity*. Agar overlay test was used to determine the antibacterial activity of UF, MF, and MMF against gram-positive bacteria (*Staphylococcus aureus*) and gram-negative bacteria (*Salmonella enterica*). A culture grown overnight at  $37^\circ\text{C}$  of each bacterial strain was re-inoculated in fresh trypticase soy broth in ratio 1:1000. This new culture was grown at 200 rpm and  $37^\circ\text{C}$  to reach an O.D. at 600 nm of 0.4. Subsequently,  $100\ \mu\text{L}$  of overnight culture was inoculated into 25 mL of non-gelified trypticase

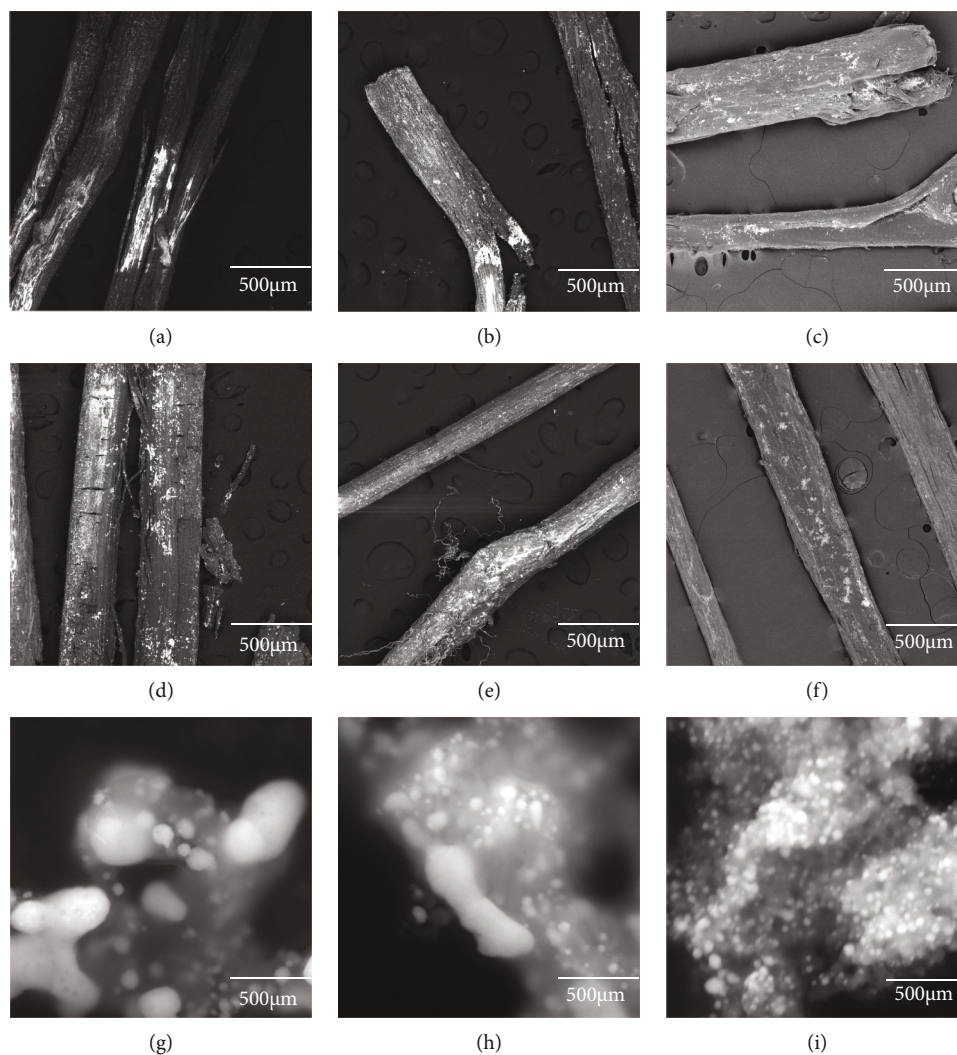


FIGURE 6: SEM images of (a) UF20, (b) MF20, (c) MMF20, (d) UF30, (e) MF30, and (f) MMF30; biosynthesized AgNPs detached from (g) UF30, (h) MF30, and (i) MMF30.

soy agar at 45°C, poured into the Petri dish, and allowed to cool until the first layer was formed. Subsequently, ATF with the different treatments were placed on the gelled agar. A new layer of agar not inoculated with the strain was placed to fix the fibers and allowed to cool until the overlaid gelled. The Petri dishes thus formed were incubated at 37°C for 16 h, and the inhibition halo was determined. The experiments were run in triplicate.

Additionally, minimum inhibitory concentrations (MICs) and percentage growth inhibition assays were performed. First, overnight cultures of *S. aureus* and *S. enterica* grown in LB broth media under agitation (250 rpm) at 37°C were done. Bacterial growth was monitored by measuring the optical density at 595 nm ( $OD_{595}$ ). Typical parameters derived from growth curves are as follows: length of lag phase ( $\lambda$ ), growth rate represented by the maximum slope ( $\mu$ ), and the maximum cell growth ( $A$ ) appears in equation (1), in which  $t$  indicates growing period and  $y_{(t)}$  indicates the growing parameter. The integral (area under the curve) is also used as growth parameter [22].

$$y_{(t)} = \frac{A}{1 + \exp((4\mu/A)(\lambda - t) + 2)}. \quad (1)$$

In a second stage, to determine the MICs at different concentrations (1, 0.5, 0.25, and 0.125 mg fiber per milliliter of LB medium) of modified fibers (MF20, MF30, MMF20, and MMF30), a modified standard MIC method was used [23]. To evaluate the lowest concentration of fiber (mg/mL) required to inhibit the visible growth of those bacterial cultures after overnight incubation (24 h), 2  $\mu$ L of each overnight culture was added to each well of a 96-well plate and allowed to incubate under agitation (250 rpm) at 37°C for 24 h. After incubation, the 96-well plate was analyzed at  $OD_{595}$ .

Percentage growth inhibition was calculated by subtracting mean OD values of respective blank from the mean OD value of an experimental set. Percentage growth in presence of compound was calculated considering the growth in the absence of any test material as 100% according to equation

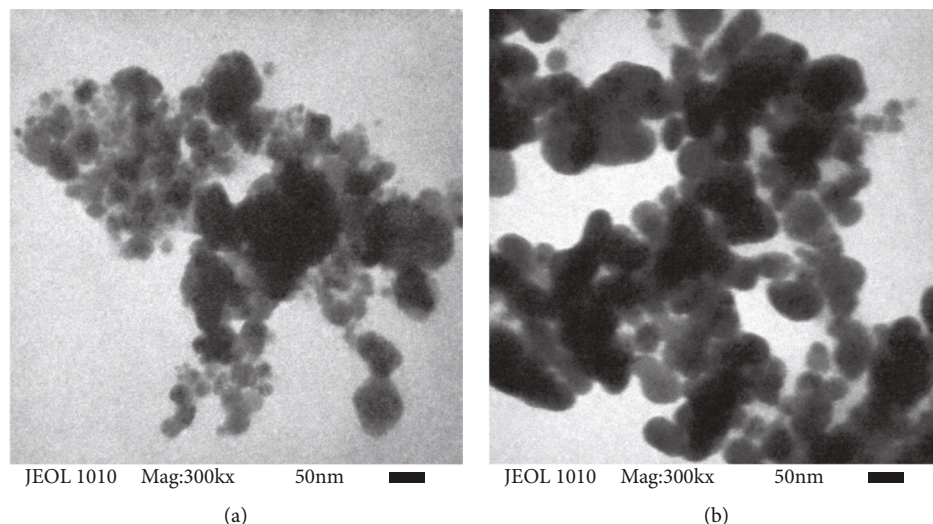


FIGURE 7: TEM images of AgNPs using  $\text{AgNO}_3$  solution as metallic precursor: (a) AgNPs20; (b) AgNPs30.

TABLE 2: Morphologies of biosynthesized AgNPs.

Plant resource	Morphology	Reference
Banana peel	Spherical	[35]
<i>Salvia spinosa</i> plant	Oval	[40]
<i>Aloe vera</i> leaf	Triangular	[41]
<i>Prunus japonica</i> leaf	Hexagonal	[42]
Orange peel	Wires, irregular, spherical	[43]
Wheat straw	Nearly spherical	[44]
Rambutan peel	Triangular and hexagonal	[45]

(2). The growth in the presence of compound was calculated by the following equation [24].

$$\text{Growth inhibition\%} = 100 - \left[ \frac{\text{OD}_{(\text{test sample})} - \text{OD}_{(\text{Blank})}}{\text{OD}_{(\text{control})} - \text{OD}_{(\text{Blank})}} \right] \times 100. \quad (2)$$

4.2. *Statistics.* Mechanical test data were analyzed with statistical software (GraphPad Software Prism 7). Data are shown as the mean and the corresponding standard error. Kruskal-Wallis test of one-way analysis of variance was performed considering tensile modulus and strength as variables. Dunn's multiple comparison test was used for the determination of statistical significance, which was defined as a value of  $p < 0.05$ .

## 5. Results and Discussion

5.1. *Agave Fibers.* The qualitative surface chemical composition of UF, MF, and MMF is presented in Figure 3. The intensity of bands around  $1030 \text{ cm}^{-1}$  commonly attributed to C-O

deformation in cellulose, symmetric C-O-C stretching, and aromatic C-H deformation of lignin, and the hydroxyl region ( $3080\text{-}3500 \text{ cm}^{-1}$ ) corresponding to wood components decreased in the following order  $\text{MF} > \text{UF} > \text{MMF}$ . As it was expected, MMF showed the lowest concentration of wood-associated chemical groups due to the use of MAPE, which completely covered wood surface. Otherwise, MF showed the highest concentration of wood-associated bands, since mercerization produced a rougher surface with a more porous structure, exposing a higher surface area to the environment [25]. On the other hand,  $\text{CH}_2$  asymmetric and symmetric bands ( $2919$  and  $2851 \text{ cm}^{-1}$ , respectively) corresponding to main absorptions of polyethylene are clearly observed only in MMF samples due to the presence of MAPE [21, 26].

Figure 4 shows SEM micrographs of treated ATF. It can be observed that MMF (Figure 4(a)) show a smooth surface, since the coupling agent (i.e., MAPE) filled the empty space between the broken fibers, producing a hydrogen-rich surface due to the presence of polyethylene. On the other hand, MF (Figure 4(b)) show a rough surface due to the removal of lignin, pectin, and hemicelluloses, which leads to fibrillation and breaking of fiber bundles exposing a heterogeneous/oxygen-rich surface structure.

Droplet formation during contact angle tests is illustrated in Figure 5; when MF were tested, an instant absorption of water upon contact area was observed (Figure 5(a)) due to the high hydrophilic nature of the fibers as a result of the mercerization process. According to reported literature [27], contact angle could not be obtained for substrates that show such behavior. Regarding MMF (Figure 5(b)), contact angle ( $\theta$ ) was calculated according to equation (3), where  $H$  corresponds to the height of a droplet and  $R$  to the radius of the droplet's base.  $\theta$  was found to be equal to  $73.72^\circ$ , indicating that the fiber treated with NaOH and MAPE (MMF) shows a less hydrophilic surface than the mercerized fiber (MF). The presence of polyethylene

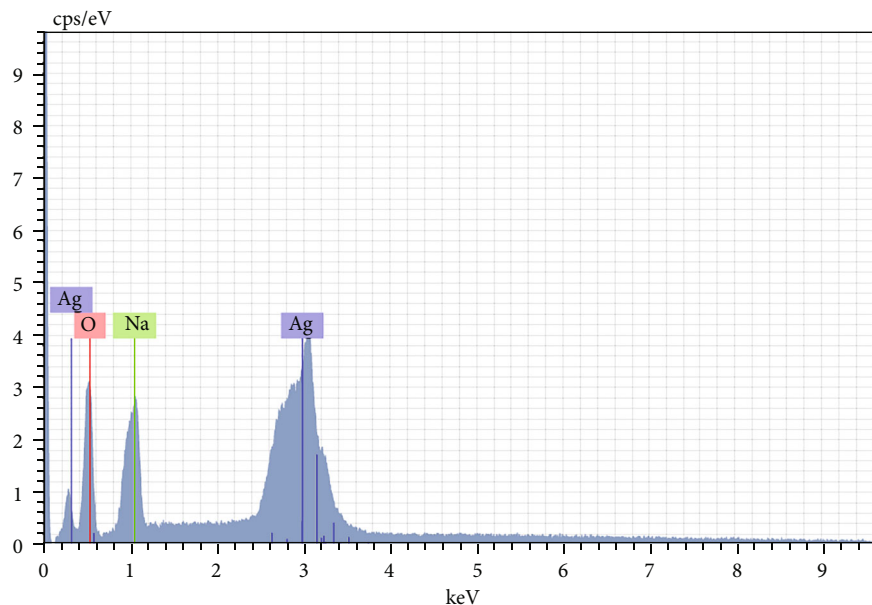


FIGURE 8: EDS spectra of AgNPs.

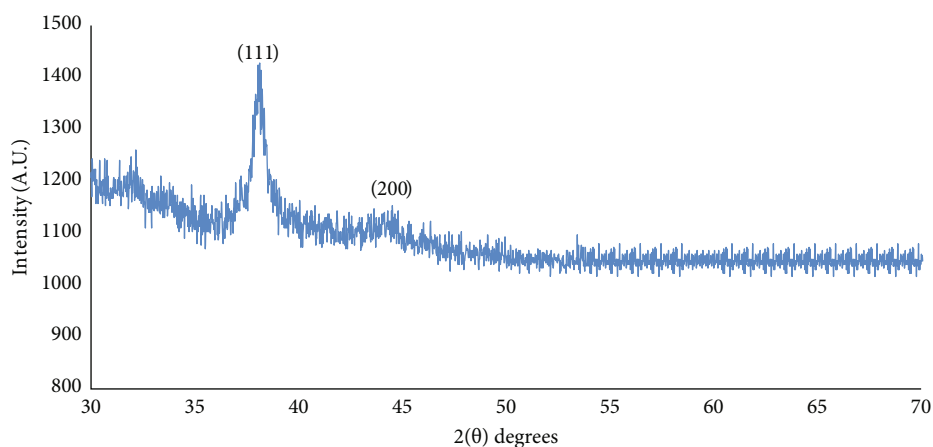


FIGURE 9: XRD patterns of biosynthesized AgNPs.

modifies the surface of the fiber due to its intrinsic hydrophobic behavior [28]. Finally, Figure 5(c) shows an image of a droplet deposited on a fiber during contact angle tests.

$$\theta = 2 * \arctan \left( \frac{H}{R} \right). \quad (3)$$

Figures 6(a)–6(f) show the SEM micrographs of UF, MF, and MMF reinforced with biosynthesized AgNPs, indicating that all samples were successfully used as templates no matter the previous surface treatment applied, since AgNPs are clearly observed on all samples. According to SEM images, there is not a defined distribution pattern of AgNPs in any type of fiber. In the case of UF and MF samples, the oxygen-rich surface structure of natural

fibers contributed to the synthesis of nanoparticles, while in the case of MMF samples, the excellent metal-binding characteristics of polyethylene promoted the superficial presence of AgNPs [21, 29]. To analyze the morphology of the biosynthesized AgNPs, particles were detached from the fibers. SEM and TEM results indicate that a wide size distribution and different shaped nanosized particles (i.e., spheres and rods) were obtained as observed in Figures 6(g)–6(i) and Figure 7, respectively, using ATE as reducing agent. So far, a wide variety of different shaped AgNPs have been synthesized as indicated in Table 2. Differences in the morphologies of biosynthesized AgNPs are due to variables such as the vast combination of biomolecules such as proteins, enzymes, polysaccharides, alkaloids, terpenoids, and vitamins obtained from different parts of the plant resources that reduce and stabilize silver ions; the reaction parameters of each

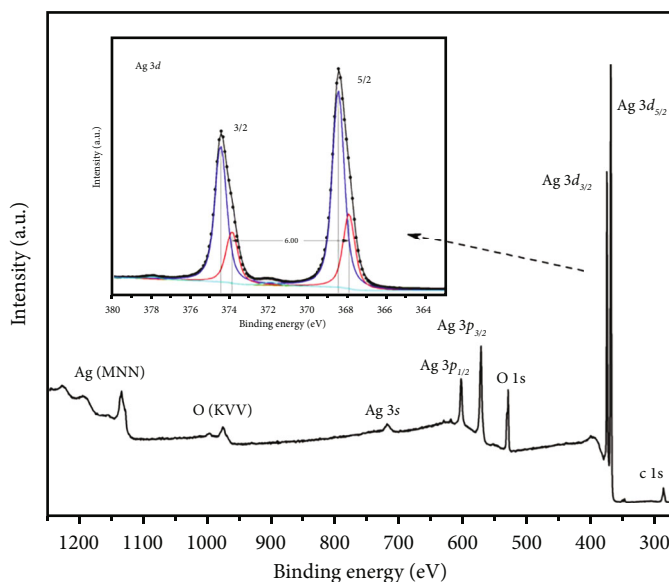


FIGURE 10: XPS survey spectra of AgNPs. Insert shows Ag3d core level spectra.

TABLE 3: DLS measurements.

Sample name	DLS	
	Average size (nm)	Z-potential (mV)
AgNPs20	135.6	-36.7
AgNPs30	112.3	-30.4

particular synthesis process (e.g., temperature, stirring, and reactant ratio); and the different synthesis methods employed (e.g., autoclave, incubator, and microwave) [8].

Regarding the surface treatment previously applied to the fiber, it seems that the heterogeneous-porous surface structure of wood promoted the formation of a wider range of morphologies as well as larger particles than the polyethylene surface of MMF produced due to the presence of MAPE. EDS analysis of detached AgNPs is shown in Figure 8. AgNPs show a strong optical absorption peak at approximately 3 keV due to their surface plasmon resonance and the following composition: silver (54.44%), oxygen (30.47%), and sodium (15.10%). The presence of sodium in silver nanoparticles may be due to the mercerization treatment of the fibers used as templates and from which the AgNPs were detached. Regarding the presence of oxygen, it could represent surface biomolecules originated from ATE [30, 31].

XRD was carried out to confirm the composition and the crystalline nature of biosynthesized AgNPs. Characteristic peaks of face cubic centered (fcc) silver corresponding to the diffraction of (111) and (200) at  $38.42^\circ$  and  $44.23^\circ$ , respectively, are shown in Figure 9. Results indicate that AgNPs showed no preferential growing direction [32].

XPS tests were performed to corroborate the nature of the biosynthesized AgNPs; results are shown in Figure 10. Main peaks observed during survey scan correspond to Ag3d, Ag3p, and O1s. Due to a high concentration of AgNPs on the film layer, the Auger zone was observed and appeared

at higher binding energy; also, the peak Ag3s is observed around 720 eV. Good intensity of three core levels, 3d, 3p, and 3s, of silver is presented, corresponding to the main cross sections of the element. The insert in Figure 8 of Ag3d shows the doublet of 3/2 and 5/2 spin orbitals. Once deconvoluted, the signal presents two components: the right component, which is positioned exactly at 367.9 eV with a splitting of 6.00 eV that corresponds to metallic silver, and the main component, positioned at 368.4 eV corresponding to  $\text{Ag}^+$  due to  $\text{Ag}_2\text{O}$  that matches with the oxygen content [33].

Table 3 shows the DLS measurements results, confirming the nanometric dimensions of the synthesized AgNPs. Moreover, the Z-potential results evidence a negative charged surface and the stability of AgNPs in water suspensions. A positive or negative charge on the surface of AgNPs gives the particle stability and prevents aggregation. According to the literature, Z-potentials higher than +30 mV or lower than -30 mV indicate very stable nanoparticles, which can preserve their structure over a long time [34]. According to DLS results, stable nanometric particles were successfully synthesized.

Tensile properties of untreated and treated ATF are presented in Table 1. Regarding UF/20 and UF/30 compared to UF, statistical analysis indicated that neither tensile strength nor tensile modulus show a significant change due to the presence of AgNPs. With respect to MF, it is clear that mercerization process produced a drop in the tensile properties compared to UF due to the fibrillation and breaking of fiber bundles. The presence of AgNPs in samples MF/20 and MF/30 did not improve significantly the tensile strength compared to MF. However, a significant improvement was observed in tensile modulus for MF/30 samples. Finally, it can also be observed that MMF show higher tensile properties compared to MF, indicating that although the presence of a coupling agent does not fully



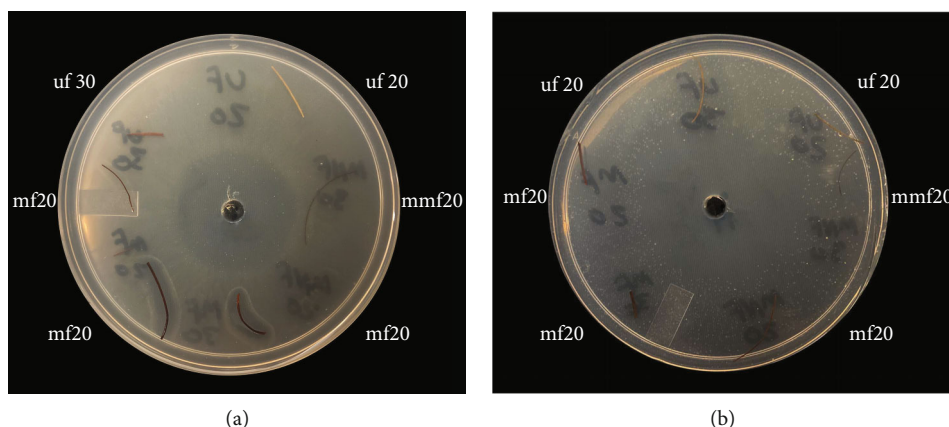


FIGURE 11: Inhibition halos obtained by the agar overlay test for analyzed samples against (a) *S. enterica* and (b) *S. aureus*.

TABLE 4: Antibacterial activity of biosynthesized AgNPs using plant extracts against different bacterial strains.

Plant resource	AgNP morphology	Bacterial strains tested	Preferentially inhibited bacteria	Reference
Banana peel	Spherical	<i>E. coli</i> (Gn)	<i>E. coli</i> (Gn) <i>P. aeruginosa</i> (Gn)	[35]
		<i>P. aeruginosa</i> (Gn)		
		<i>B. subtilis</i> (Gp) <i>S. aureus</i> (Gp)		
<i>Tectona grandis</i> seeds	Spherical	<i>B. cereus</i> (Gp)	<i>E. coli</i> (Gn)	[37]
		<i>S. aureus</i> (Gp)		
		<i>E. coli</i> (Gn)		
<i>Thymus kotschyanus</i> plant	Spherical	<i>S. aureus</i> (Gp)	<i>E. coli</i> (Gn) <i>P. aeruginosa</i> (Gn)	[46]
		<i>B. subtilis</i> (Gp)		
		<i>E. coli</i> (Gn)		
<i>Boerhaavia diffusa</i> plant	Spherical	<i>P. aeruginosa</i> (Gn)	<i>F. branchiophilum</i> (Gn)	[47]
		<i>A. hydrophila</i> (Gn)		
		<i>P. fluorescens</i> (Gn) <i>F. branchiophilum</i> (Gn)		
<i>Moringa oleifera</i> leaf	Spherical	<i>S. aureus</i> (Gp)	<i>E. coli</i> (Gn) <i>K. pneumoniae</i> (Gn)	[31]
		<i>E. faecalis</i> (Gp)		
		<i>E. coli</i> (Gn)		
		<i>K. pneumoniae</i> (Gn)		
		<i>P. aeruginosa</i> (Gn)		

Gn: gram negative; Gp: gram positive.

compensate the negative effect of mercerization, it certainly reinforces the fiber and helps to restore its original properties. Furthermore, the presence of AgNPs significantly improved both, tensile strength and modulus of MMF. According to Dunn's tests, in the case of tensile modulus, a significant improvement was observed for MMF/20 and MMF/30 samples. On the other hand, tensile strength showed a significant change in the case of MMF/30 samples. In light of the registered micrographs and the obtained tensile results, the hydrophobic surface of MMF compared to the hydrophilic surface of both UF and MF promoted the synthesis of comparatively smaller nanoparticles, which were more homogeneously distributed in the MMF system, resulting in a better attachment of AgNPs due to hydrophobic interactions and, consequently, in a more notorious effect on the mechanical behavior.

The antibacterial activity was evaluated against different gram-positive and gram-negative bacteria (Figure 11). Biosynthesized AgNPs were found to inhibit the growth of *S. enterica* as shown in Figure 11(a). It can be clearly observed the inhibition halos corresponding to MF/20, MF/30, MMF/20, and MMF/30 due to the presence of AgNPs. It is known that Ag breakdown bacteria cell wall, inhibiting intracellular enzyme activity, since AgNPs are attached to ATF, the inhibition halo is produced due to the releasing of Ag ions to the agar medium [21]. In our experiments, we could not find antimicrobial activity against the gram-positive bacteria evaluated, *S. aureus* (Figure 11(b)); however, it is known that among the mechanisms of action of AgNPs for the inhibition of bacterial growth, gram-negative bacteria are usually more susceptible due to their own morphological characteristics and cell wall composition. In the case of gram-

positive bacteria, a rigid cell wall composed of a thick layer of peptidoglycan consisting of polysaccharide chains cross linked by short peptides is observed, whereas in the case of gram-negative bacteria, the presence of a thinner layer (i.e., less rigid cell wall) of peptidoglycan facilitates the penetration of AgNPs [35–37]. A comparison of our results and those of some other works regarding the antibacterial activity of biosynthesized AgNPs using plant extracts against different bacterial strains is provided in Table 4. It can be observed that gram-negative bacteria are preferentially inhibited by AgNPs. On the other hand, the variation observed in the inhibition halos is a natural process of fiber treatments; other authors have reported that the change in the distribution of nanoparticles on the fiber can affect the release of these to achieve bacterial inhibition [38, 39].

Regarding minimum inhibitory concentration (MIC) and percentage growth inhibition, the modified fibers showed inhibitory specificity against *S. enterica*. In the case of MF20, MF30, and MMF20 samples, a MIC of 0.5 mg of the fiber per milliliter of LB medium can inhibit up to 50% of the bacterial growth. In the case of MMF30, an MIC of 0.25 mg of fiber/mL of medium was able to inhibit the growth bacteria up to 60%.

However, despite observing that these modified fibers could have great inhibitory activity in the growth rate of gram-negative bacteria, for the gram-positive bacteria such *S. aureus* did not show a significant change in the rate of percentage growth. This suggests that the MIC could be above the concentration of 1 mg/mL or definitively does not have inhibitory action on the bacterial growth of *S. aureus*.

## 6. Conclusions

In the present work, the effect of biosynthesized AgNPs on the properties of surface-modified ATF was evaluated. Results indicate that the presence of AgNPs significantly increased the tensile modulus and strength of mercerized fibers treated with MAPE, especially in the case of MMF/30 samples. A less hydrophilic surface caused by the presence of polyethylene could have promoted a better attachment of AgNPs to AT fibers. AgNPs also conferred antibacterial properties to MF and MMF due to the presence of Ag ions. XRD and XPS results confirm the composition of the synthesized particles. SEM, TEM, and DLS results indicate that stable nanometric particles were successfully obtained.

## Data Availability

Data will be available on request (contact information: Edgar López, edgar.lopez@academicos.udg.mx).

## Conflicts of Interest

The authors declare no conflicts of interest.

## Acknowledgments

The authors want to thank Sergio Oliva-León and Ricardo Martínez-Magallanes for their technical support. This work was supported by the Centro de Ciencias Exactas e Ingenierías Universidad de Guadalajara.

## References

- [1] A. Constante, S. Pillay, H. Ning, and U. K. Vaidya, "Utilization of algae blooms as a source of natural fibers for biocomposite materials: study of morphology and mechanical performance of Lyngbya fibers," *Algal Research*, vol. 12, pp. 412–420, 2015.
- [2] A. Oushabi, S. Sair, F. Oudrhiri Hassani, Y. Abboud, O. Tanane, and A. el Bouari, "The effect of alkali treatment on mechanical, morphological and thermal properties of date palm fibers (DPFs): study of the interface of DPF- polyurethane composite," *South African Journal of Chemistry*, vol. 23, pp. 116–123, 2017.
- [3] R. Sepe, F. Bollino, L. Boccarusso, and F. Caputo, "Influence of chemical treatments on mechanical properties of hemp fiber reinforced composites," *Composites Part B Engineering*, vol. 133, pp. 210–217, 2018.
- [4] M. Sood, D. Deepak, and V. K. Gupta, "Effect of fiber chemical treatment on mechanical properties of sisal fiber/recycled HDPE composite," *Materials Today*, vol. 2, pp. 3149–3155, 2015.
- [5] A. El-Sabbagh, "Effect of coupling agent on natural fibre in natural fibre/polypropylene composites on mechanical and thermal behaviour," *Composites Part B Engineering*, vol. 57, pp. 126–135, 2014.
- [6] Z. Shen, Z. Ye, K. Li, and C. Qi, "Effects of coupling agent and thermoplastic on the interfacial bond strength and the mechanical properties of oriented wood strand-thermoplastic composites," *Polymers*, vol. 13, no. 4260, pp. 1–11, 2021.
- [7] D. Baruah, R. N. S. Yadav, A. Yadav, and A. M. Das, "Alpinia nigra fruits mediated synthesis of silver nanoparticles and their antimicrobial photocatalytic activities," *Journal of Photochemistry and Photobiology. B*, vol. 201, pp. 111649–111657, 2019.
- [8] S. Ahmed, M. Ahmad, B. L. Swami, and S. Ikram, "A review on plants extract mediated synthesis of silver nanoparticles for antimicrobial applications: a green expertise," *Journal of Advanced Research*, vol. 7, no. 1, pp. 17–28, 2016.
- [9] D. K. Poudel, P. Niraula, H. Aryal et al., "Plant-mediated green synthesis of Ag NPs and their possible applications: a critical review," *J Nanotechnol*, vol. 2022, pp. 1–24, 2022.
- [10] F. Rodríguez-Félix, A. Z. Graciano-Verdugo, M. J. Moreno-Vásquez et al., "Trends in sustainable green synthesis of silver nanoparticles using agri-food waste extracts and their applications in health," *Journal of Nanomaterials*, vol. 2022, 37 pages, 2022.
- [11] S. Adewale Akintelu, Y. Bo, and A. Similoluwa Folorunso, "A review on synthesis, optimization, mechanism, characterization, and antibacterial application of silver nanoparticles synthesized from plants," *Journal of Chemistry*, vol. 2020, 12 pages, 2020.
- [12] N. R. Chowdhury, M. MacGregor-Ramiasa, P. Zilm, P. Majewski, and K. Vasilev, "'Chocolate' silver nanoparticles: synthesis, antibacterial activity and cytotoxicity," *Journal of Colloid and Interface Science*, vol. 482, pp. 151–158, 2016.
- [13] P. Kuppusamy, M. M. Yusoff, G. P. Maniam, and N. Govindan, "Biosynthesis of metallic nanoparticles using plant derivatives and their new avenues in pharmacological

- applications - an updated report," *Saudi Pharm J*, vol. 24, no. 4, pp. 473–484, 2016.
- [14] M. Jannathul Firdhouse and P. Lalitha, "Biosynthesis of silver nanoparticles and its applications," *J Nanotechnol*, vol. 2015, pp. 1–18, 2015.
- [15] I. H. Hilal, M. R. Mohammed, and W. A. Shakir, "Effect of silver (Ag) nanoparticles on structural and mechanical properties of (PMMA) blend and its application for denture base," *Int J Med Res Health Sci*, vol. 8, no. 1, pp. 154–159, 2019.
- [16] A. A. Issa, M. al-Maadeed, A. Luyt, D. Ponnamma, and M. Hassan, "Physico-mechanical, dielectric, and piezoelectric properties of PVDF electrospun mats containing silver nanoparticles," *J Carbon Res*, vol. 3, no. 4, pp. 30–45, 2017.
- [17] A. Adeodu, L. Mudashiru, I. Daniyan, and A. Awodoyin, "Effect of silver nanoparticle (AgNP) mixed with calcium carbonate on impact, hardness and tensile strength properties of aluminium 6063," *Journal of Composite Materials*, p. 002199832092314, 2020.
- [18] T. Y. Suzuki, J. Gallego, W. G. Assunção, A. L. Briso, and P. H. Dos Santos, "Influence of silver nanoparticle solution on the mechanical properties of resin cements and intrarradicular dentin," *PLoS One*, vol. 14, no. 6, p. e0217750, 2019.
- [19] A. I. Alejandro, V. O. Adolfo, R. L. Ericka, M. Valery, R. H. Alejandrina, and C. S. Jesús, "Interaction of green silver nanoparticles on mechanical properties of the rat skeletal muscle," *Journal of Nanoscience and Nanotechnology*, vol. 17, no. 12, pp. 9172–9175, 2017.
- [20] C. H. Su, H. L. Chen, S. P. Ju et al., "The mechanical behaviors of polyethylene/silver nanoparticle composites: an insight from molecular dynamics study," *Scientific Reports*, vol. 10, no. 7600, pp. 1–14, 2020.
- [21] R. A. Morales-Luckie, A. A. Lopezfuentes-Ruiz, O. F. Olea-Mejía et al., "Synthessi of silver nanoparticles using aqueous extracts of *Heterotheca inuloides* as reducing agent and natural fibers as templates: *Agave lechugilla* and silk," *Materials Science and Engineering: C*, vol. 69, pp. 429–436, 2016.
- [22] M. Kahm, G. Hasenbrink, H. Lichtenberg-Fraté, J. Ludwig, and M. Kschischo, "Growthfit: fitting biological growth curves with R," *Journal of Statistical Software*, vol. 33, pp. 1–21, 2015.
- [23] J. M. Andrews, "Determination of minimum inhibitory concentrations," *The Journal of Antimicrobial Chemotherapy*, vol. 48, suppl\_1, pp. 5–16, 2001.
- [24] D. J. Paul, N. B. Laure, S. K. Guru et al., "Antiproliferative and antimicrobial activities of alkylbenzoquinone derivatives from *Ardisia kivuensis*," *Pharmaceutical Biology*, vol. 52, no. 3, pp. 392–397, 2014.
- [25] M. Sood, D. Deepak, and V. K. Gupta, "Effect of fiber chemical treatment on mechanical properties of sisal fiber/recycled HDPE composite," *Materials Today*, vol. 2, no. 4-5, pp. 3149–3155, 2015.
- [26] C. Zhu, J. Xue, and J. He, "Controlled in-situ synthesis of silver nanoparticles in natural cellulose fibers toward highly efficient antimicrobial materials," *Journal of Nanoscience and Nanotechnology*, vol. 9, no. 5, pp. 3067–3074, 2009.
- [27] N. A. Rosli, I. Ahmad, I. Abdullah, F. H. Anuar, and F. Mohamed, "Hydrophobic modification of cellulose isolated from *Agave angustifolia* fibre by graft copolymerisation using methyl methacrylate," *Carbohydrate Polymers*, vol. 125, pp. 69–75, 2015.
- [28] L. Silvia, I. Hasanah, and M. Zainuri, "Hydrophobic of Polyethylene/SiO<sub>2</sub> Modified Coating for Self Cleaing Material," in *International conference on science and applied science (ICSAS)*, AIP Publishing, Surakarta, 2019.
- [29] A. R. Abbasi, H. Kalantary, M. Yousefi, A. Ramazani, and A. Morsali, "Synthesis and characterization of Ag [email protected] fibers under ultrasound irradiation," *Ultrasonics Sonochemistry*, vol. 19, no. 4, pp. 853–857, 2012.
- [30] S. Fatema, M. Shirsat, M. Farooqui, and M. A. Pathan, "Biosynthesis of silver nanoparticle using aqueous extract of *Saraca asoca* leaves, its characterization and antimicrobial activity," *Int J Dimens*, vol. 10, no. 2, pp. 163–168, 2019.
- [31] J. S. Moodley, S. B. N. Krishna, K. Pillay, Sershen, and P. Govender, "Green synthesis of silver nanoparticles from *Moringa oleifera* leaf extracts and its antimicrobial potential," *Advances in Natural Sciences: Nanoscience and Nanotechnology*, vol. 9, no. 1, pp. 1–10, 2018.
- [32] E. J. López-Naranjo, I. P. Hernández-Rosales, A. Y. Buenodurán et al., "Biosynthesis of silver nanoparticles using a natural extract obtained from an agroindustrial residue of the tequila industry," *MaterLett*, vol. 213, pp. 278–281, 2018.
- [33] A. Herrera-Gómez, "Uncertainties in photoemission peak fitting accounting for the covariance with background parameters," *Journal of Vacuum Science and Technology A*, vol. 38, no. 3, article 033211, 2020.
- [34] O. Erdogan, M. Abbak, G. M. Demirbolat et al., "Green synthesis of silver nanoparticles via *Cynara scolymus* leaf extracts: the characterization, anticancer potential with photodynamic therapy in MC7 cells," *PLoS One*, vol. 14, no. 6, pp. 1–15, 2019.
- [35] H. M. M. Ibrahim, "Green synthesis and characterization of silver nanoparticles using banana peel extract and their antimicrobial activity against representative microorganisms," *Journal of Radiation Research and Applied Science*, vol. 8, no. 3, pp. 265–275, 2015.
- [36] Y. N. Slavin, J. Asnis, U. O. Häfeli, and H. Bach, "Metal nanoparticles: understanding the mechanisms behind antibacterial activity," *J Nanobiotechnology*, vol. 15, no. 1, pp. 1–20, 2017.
- [37] A. Rautela, J. Rani, and M. Debnath, "Green synthesis of silver nanoparticles from *Tectona grandis* seeds extract: characterization and mechanism of antimicrobial action on different microorganisms," *Journal of Analytical Science and Technology*, vol. 10, no. 1, pp. 1–10, 2019.
- [38] G. Montes-Hernandez, M. Di Girolamo, G. Sarret et al., "In situ formation of silver nanoparticles (Ag-NPs) onto textile fibers," *ACS Omega*, vol. 6, no. 2, pp. 1316–1327, 2021.
- [39] E. Smiechowicz, B. Niekraszewicz, P. Kulpinski, and K. Dzitko, "Antibacterial composite cellulose fibers modified with silver nanoparticles and nanosilica," *Cellulose*, vol. 25, no. 6, pp. 3499–3517, 2018.
- [40] P. Saba, G. Maryam, and B. Saeid, "Green synthesis of silver nanoparticles using the plant extract of *Salvia spinosa* grown in vitro and their antibacterial activity assessment," *Journal of Nanostructure in Chemistry*, vol. 9, no. 1, pp. 1–9, 2019.
- [41] S. Medda, A. Hajra, U. Dey, P. Bose, and N. K. Mondal, "Biosynthesis of silver nanoparticles from *Aloe vera* leaf extract and antifungal activity against *Rhizopus* sp and *Aspergillus* sp," *Applied Nanoscience*, vol. 5, no. 7, pp. 875–880, 2015.
- [42] A. Saravanakumar, M. M. Peng, M. Ganesh, J. Jayaprakash, M. Mohankumar, and H. T. Jang, "Low-cost and eco-friendly green synthesis of silver nanoparticles using *Prunus japonica* (Rosaceae) leaf extract and their antibacterial, antioxidant properties," *Artif Cells Nanomed Biotechnol*, vol. 45, no. 6, pp. 1–7, 2017.

- [43] L. Castro, M. L. Blázquez, F. González, J. Á. Muñoz, and A. Ballester, "Biosynthesis of silver and platinum nanoparticles using orange peel extract: characterisation and applications," *IET Nanobiotechnology*, vol. 9, no. 5, pp. 252–258, 2015.
- [44] Q. Ma, J. Li, L. Xu, Q. Sun, B. Yong, and Y. Wang, "Biosynthesis of silver nanoparticles using wheat straw biomass under light radiation and their antibacterial activity," *BioResources*, vol. 11, no. 4, pp. 10190–10200, 2016.
- [45] B. Kumar, K. Smita, L. Cumbal, and Y. Angulo, "Fabrication of silver nanoplates using *Nephelium lappaceum* (Rambutan) peel: a sustainable approach," *Journal of Molecular Liquids*, vol. 211, pp. 476–480, 2015.
- [46] M. Hamelian, M. M. Zangeneh, A. Amisama, K. Varmira, and H. Veisi, "Green synthesis of silver nanoparticles using *Thymus kotschyanus* extract and evaluation of their antioxidant, antibacterial and cytotoxic effects," *Applied Organometallic Chemistry*, vol. 4458, pp. 1–8, 2018.
- [47] P. V. Kumar, S. V. Pammi, P. Kollu, K. V. Satyanarayana, and U. Shameem, "Green synthesis and characterization of silver nanoparticles using *Boerhaavia diffusa* plant extract and their antibacterial activity," *Ind Crops Prods*, vol. 52, pp. 562–566, 2014.